TOPICAL REVIEW — Iron-based high temperature superconductors

Microstructure and structural phase transitions in iron-based superconductors*

Wang Zhen(王 臻), Cai Yao(蔡 瑶), Yang Huai-Xin(杨槐馨), Tian Huan-Fang(田焕芳), Wang Zhi-Wei(王秩伟), Ma Chao(马 超), Chen Zhen(陈 震), and Li Jian-Qi(李建奇)†

Beijing National Laboratory for Condensed Matter Physics, Institute of Physics, Chinese Academy of Sciences, Beijing 100190, *China*

(Received 23 April 2013)

Crystal structures and microstructural features, such as structural phase transitions, defect structures, and chemical and structural inhomogeneities, are known to have profound effects on the physical properties of superconducting materials. Recently, many studies on the structural properties of Fe-based high-T_c superconductors have been published. This review article will mainly focus on the typical microstructural features in samples that have been well characterized by physical measurements. (i) Certain common structural features are discussed, in particular, the crystal structural features for different superconducting families, the local structural distortions in the Fe_2Pn_2 (*Pn* = P, As, Sb) or Fe_2Ch_2 (*Ch* = S, Se, Te) blocks, and the structural transformations in the 122 system. (ii) In FeTe(Se) (11 family), the superconductivity, chemical and structural inhomogeneities are investigated and discussed in correlation with superconductivity. (iii) In the $K_{0.8}Fe_{1.6+x}Se_2$ system, we focus on the typical compounds with emphasis on the Fe-vacancy order and phase separations. The microstructural features in other superconducting materials are also briefly discussed.

Keywords: Fe-based superconductor, structural transition, structural inhomogeneity, phase separation

PACS: 74.70.Xa, 61.05.J–, 61.50.Ks, 61.72.–y **DOI:** 10.1088/1674-1056/22/8/087409

1. Introduction

The discovery of superconductivity in F-doped LaOFeAs[1] with $T_c = 26$ K following an earlier report of superconductivity in $LaFePO_{1-x}F_x$[2] has stimulated renewed interest in the investigation of high-T_c superconductors. Materials containing iron have always been considered a challenge for obtaining a superconducting transition at high temperature because of the antagonistic properties between superconductivity and magnetism. Soon after this discovery, a number of superconducting families with T_c ranging from 2 K to 56 K were obtained,[3–7] such as *Ln*FeAsO (*Ln* = rare earth metal, such as La and Sm) with a ZrCuSiAs structure (so-called 1111 type). Moreover, Sm substitution for La in the 1111 structure can raise T_c up to 55 K.[7] In addition to the 1111 system, other families of Fe-based superconductors are found to show a rich variety of structural and physical properties, including $A_EFe_2As_2$ (A_E = alkali-earth metals) with a $ThCr_2Si_2$ structure (122 type),[8–11] *A*FeAs (*A* = Li, Na) with a Cu_2Sb structure (111 type),[12–15] and FeSe with a PbO structure (11 type).[16,17] Recently, experimental investigations have also demonstrated that the intercalation of additional layers into this kind of layered system can create new materials with superconductivity.[18–21] For example, $Sr_2VFeAsO_3$ (21113 type)[20] and $Sr_3Sc_2Fe_2As_2O_5$ (32225 type)[21] contain intercalated perovskite-like blocks and exhibit superconductivity at around 37 K and 45 K, respectively. Superconductivity in $K_yFe_{1.6+x}Se_2$ was discovered in 2010,[22] and then experimental measurements in related systems showed that these types of materials, e.g., $Rb_xFe_{2-y}Se_2$, $Cs_xFe_{2-y}Se_2$, (Tl, K)$_x$Fe$_y$Se$_2$, and (Rb, K)$_x$Fe$_y$Se$_2$, often have a T_c ranging from 28 K to 32 K depending on the chemical composition.[23–26] The basic structures of $A_{0.8}Fe_{1.6+x}Se_2$ (*A* = K, Rb, Cs, Tl/K, Tl/Rb) superconductors show certain similar properties to the 122 system, which has a space group of *I*4/*mmm*. In addition, the presence of Fe-vacancy ordering within the FeSe layer is observed commonly in this layered system, so it was called the 122* type structure in the previous literature. Compared with other Fe-based superconductors, the 122* system exhibits some remarkable physical and structural properties. For instance, the superconducting volume in most samples is only about 20%, as estimated from the magnetic shielding data obtained under high applied fields. Moreover, the 122* materials often show complex microstructural features arising from Fe-vacancy orders and phase separations. In this article, we will focus on the crystal structures and microstructural features observed in a number of Fe-based superconducting systems, such as structural transformations, defect structures, chemical and structural inhomogeneities. These structural phenomena are considered to have profound effects on the physical properties of superconducting materials.

*Project supported by the National Basic Research Program of China (Grant Nos. 2011CBA00101, 2010CB923002, 2011CB921703, and 2012CB821404), the National Natural Science Foundation of China (Grant Nos. 11274368, 51272277, 11074292, 11004229, and 11190022), and the Chinese Academy of Sciences.

†Corresponding author. E-mail: LJQ@aphy.iphy.ac.cn

© 2013 Chinese Physical Society and IOP Publishing Ltd

2. Some fundamental results of Fe-based superconductor structures

In general, Fe-based superconductors adopt layered structures, and the essential layers, i.e., the Fe_2Pn_2 (Pn = P, As, Sb) or Fe_2Ch_2 (Ch = S, Se, Te) blocks, play a critical role in the appearance of superconductivity in this kind of material. Experimental investigations demonstrate that these blocks can stack up in a number of different ways in superconducting materials. For instance, intercalated layers (A) between Fe_2Pn_2 layers following a sequence of ...[Fe_2Pn_2]/A/[Fe_2Pn_2]/A/[Fe_2Pn_2]... results in 122-type superconductors, as commonly discussed in the previous investigations. Figure 1 shows a series of structural models, schematically illustrating the basic crystal structures of the observed superconducting families. The quasi-two-dimensional Fe_2Pn_2/Ch_2 block consists of a square lattice of iron atoms with Pn/Ch atoms coordinating at the apical sites. High-resolution transmission electron microscopy (TEM) observations along the relevant directions clearly reveal the atomic structural features in all structural layers. Figure 2 exhibits a high-resolution TEM image taken from a $SrFe_2As_2$ crystal along the [100] zone-axis direction, illustrating the visible atomic layers stacking along the c-axis direction.[27]

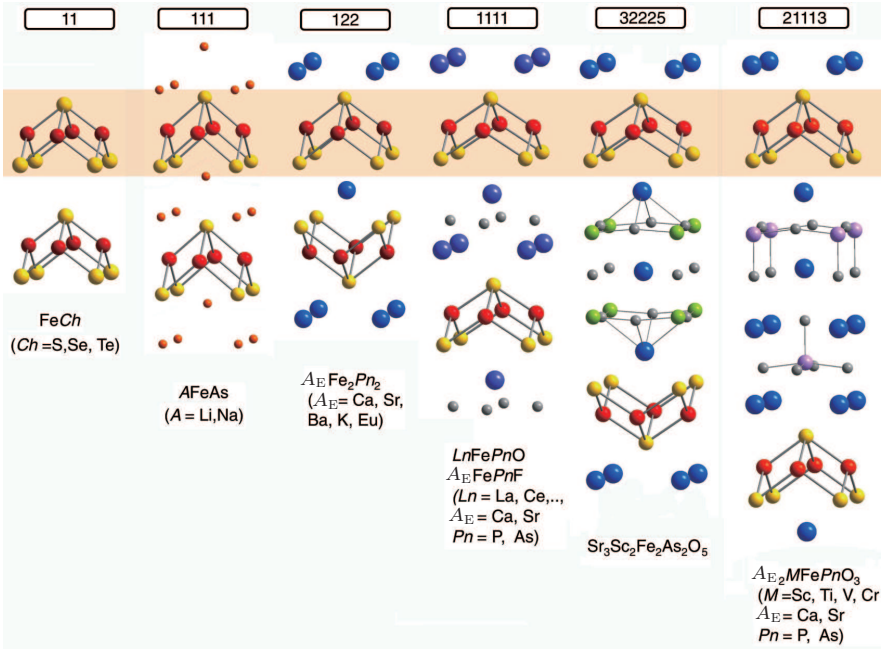


Fig. 1. The crystal structures of Fe-based superconductors with 11-, 111-, 122-, 1111-, 21113-, and 32225-type structures. The FeCh/FePn (Pn: pnictogen, Ch: chalcogen) tetragonal blocks are highlighted in these structural models.

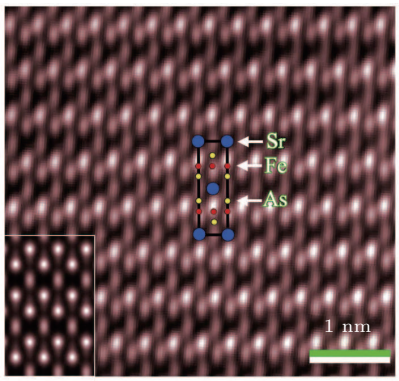


Fig. 2. High-resolution TEM image of $SrFe_2As_2$ taken along the [100] zone-axis direction, illustrating the layered structural features, and a theoretical simulated image is superimposed for comparison.[27]

The FePn/Ch layers in the Fe-based compounds, as discussed similarly for the CuO_2 plane in the Cu-based superconductors, also play a key role in understanding the superconductivity. The geometric structural features of the FePn/Ch blocks are essentially in correlation with the magnetic orders and electronic properties of these materials due to the strong bonding between Fe–Fe and Fe–Pn/Ch. The ground state of Cu-based superconductors has a long-range antiferromagnetic (AFM) order with the Cu spins aligned as shown in Fig. 3(a).[28,29] It is notable that certain Fe-based superconductors also exhibit a similar magnetic order in the a–b basic plane, as illustrated in Fig. 3(b), in which the spins of neighboring Fe ions are arranged ferromagnetically along one chain and antiferromagnetically along the other direction in the orthorhombic structure. This type of magnetic structure is called collinear AFM order. The magnetic structure along the c axis can be ordered either ferromagnetically or antiferromagnetically depending on the crystal structure and intercalated layers.[30,31] On the other hand, theoretical calculations and experimental measurements demonstrate that the magnetic ground state of FeTe has a bi-collinear AFM order, as presented in Fig. 3(c).[32,33]

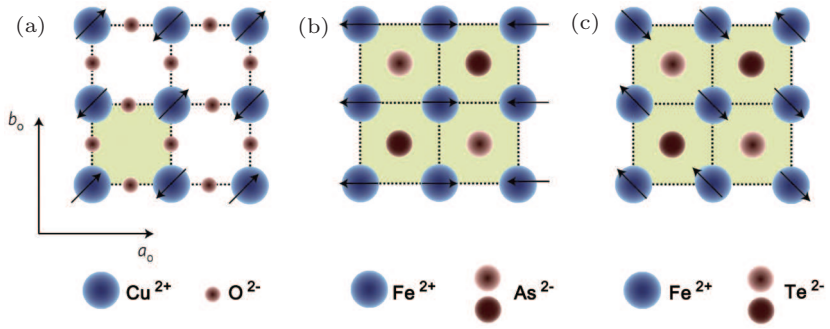


Fig. 3. The magnetic orders within the basic a–b plane for some of the parent phases: (a) La_2CuO_4, (b) $BaFe_2As_2$, and (c) FeTe. The chemical unit cells are marked as light green. The dark and light brown As/Te/Se atoms indicate their vertical positions above and below the Fe layer, respectively.[29]

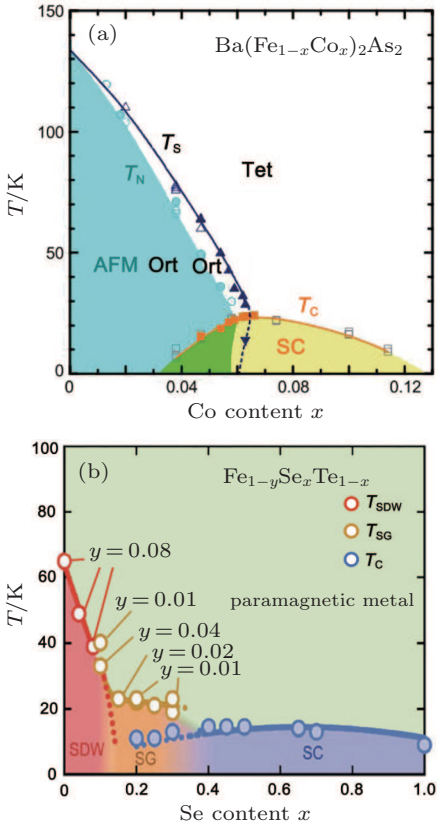


Fig. 4. Phase diagrams for iron-based superconductors of (a) $Ba(Fe_{2-x}Co_x)_2As_2$ and (b) $FeTe_{1-x}Se_x$.[36,37]

It is also noted that the superconductivity and magnetic orders in Fe-based compounds can evidently be affected by local structural distortion, which can be tuned through chemical substitution and element doping. Doping at different sites in the 122 and 1111 systems could eventually suppress the structural distortion and related spin density wave (SDW) order,[34,35] and then lead to the appearance of superconductivity. For instance, a small fraction of Co substitution for Fe could result in rich physical and structural properties in $BaFe_{2-x}Co_2As_2$. Figure 4(a) shows a phase diagram clearly illustrating the transition of the AFM state into superconductivity following Co-doping on the Fe sites.[36] For $FeTe_{1-x}Se_x$ compounds (11 system), FeTe has a tetragonal structure and shows evident monoclinic distortion accompanied by an SDW state at low temperatures, as shown in Fig. 4(b).[37] With Se substitution for Te, the crystal structure at low temperatures changes from a monoclinic to orthorhombic lattice, which could be in favor of superconductivity. It is commonly noted that the maximum superconducting critical temperature is reached only when the structural distortion and magnetic order are completely suppressed.

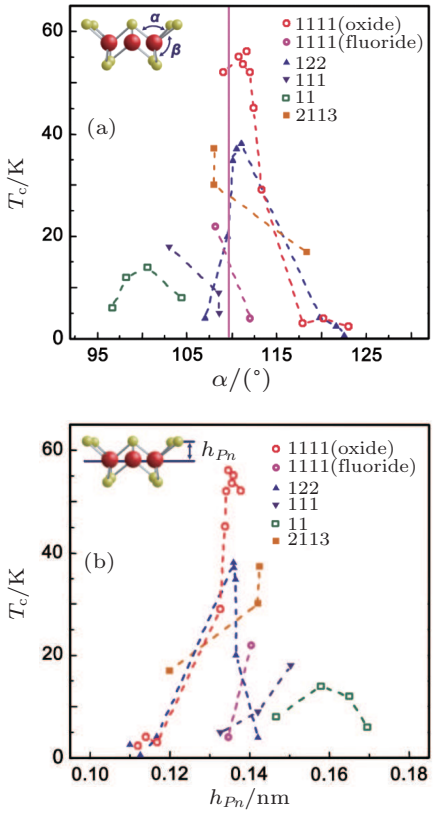


Fig. 5. (a) Superconducting T_c versus the $Pn(Ch)$–Fe–$Pn(Ch)$ angle in a number of systems. (b) Superconducting T_c versus anion height ($h_{Pn/Ch}$) in iron pnictide and iron chalcogenide blocks.[38]

Actually, the effects of the local structural features on superconductivity in Fe-based superconductors have been extensively investigated in the recent studies, and certain theoretical discussions and experimental results have been summarized in the previous literature.[38–40] It is widely accepted

that the maximum T_c favors an undistorted $Pn(Ch)$Fe$Pn(Ch)$ octahedron with an ideal Fe–$Pn(Ch)$ bond angle of 109.47°. Figure 5(a) shows the experimental results obtained in a variety of superconducting systems, in which the superconducting T_c versus the $Pn(Ch)$–Fe–$Pn(Ch)$ angle is plotted.[41] On the other hand, the superconducting T_c can be raised with the increase in the height from the $Pn(Ch)$ to Fe plane ($h_{Pn/Ch}$) in the same block. Figure 5(b) shows the experimental results obtained from a few typical superconducting systems, demonstrating the evident effects of h_{pn} on the superconductivity in Fe-based superconductors.[39–41] Moreover, Ogino's group reported that T_c in iron pnictides can be increased slightly with the rise in thickness of the Fe–$Pn(Ch)$ blocks, but saturates at a thickness of around ~ 1.5 nm.[41]

3. Structural phase transition in the 122 system

In general, the $A_EFe_2As_2$ (A_E= Sr, Ca, Ba) materials show visible structural transitions at low temperatures; the anomalies of electrical resistivity and magnetic susceptibility in 122 materials are found to be associated with the SDW instability and tetragonal ($I4/mmm$) to orthorhombic ($Fmmm$) (T–O) phase transition at low temperatures.[11,30,42] We herein illustrate the structural changes in correlation with the T–O phase transition as directly observed in $BaFe_2As_2$ and $CaFe_2As_2$ compounds by means of *in-situ* cooling TEM experiments from room temperature (RT) down to 20 K.[27]

The $SrFe_2As_2$ compound undergoes a structural transition at about 250 K, associated with SDW instability.[30] As can be seen in Figs. 6(a)–6(c), the bright-field image and corresponding selected area electron diffraction (DPs) show the typical structural changes through the T–O phase transition, illustrating the twinning lamellae in the low-temperature orthorhombic phase, which is heavily twinned with the $(110)_{orth}$ twinning plane. Different space groups are used in the present studies to describe the two structures: the a and b axis directions in the low-temperature orthorhombic phase refer to the [110] and [-110] directions in comparison with the room-temperature tetragonal phase. The width of the twin domains ranges from 100 nm to 400 nm at 100 K, and the twin density can be affected by thermal processes, impurity contents, and sample preparation techniques, as we discussed in Ref. [43]. In Fig. 6(d), we propose a schematic structural model of the mirrored twinning structure in the Fe layer. The spot splitting along the $\langle 110\rangle_{orth}$ direction with an angle of $\sim 0.1°$ in the DPs obtained from several twin domains in Fig. 6(c) indicates the ratio of the lattice parameter a/b to be about 1.009, which is fundamentally in agreement with the data of the X-ray and neutron diffractions 1.010.[44] The relationship between the magnetic state and the twinning structure that widely exists in the low-temperature orthorhombic phase is an open question currently under investigation.

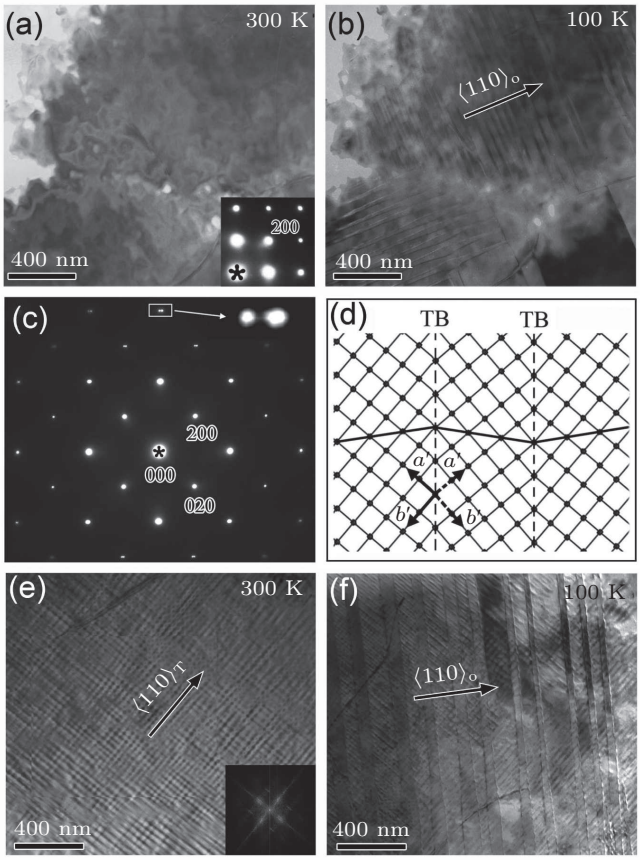


Fig. 6. The structural changes accompanying the T–O transition for 122 parent compounds. Bright-field images for the $SrFe_2As_2$ sample at (a) 300 K and (b) 100 K with a twinning structure, and (c) the electron-diffraction patterns taken along the [001] zone-axis direction at 100 K. The inset shows the enlarged (400) Bragg spot splitting along the $\langle 110\rangle_{orth}$ direction. (d) Structural model schematically illustrating the twin boundaries within an Fe layer; here TB represents the twin boundary. (e) Bright-field TEM image of $CaFe_2As_2$ at room temperature, showing a tweed structure induced by pseudoperiodic modulation along the $\langle 110\rangle_{tetra}$ direction. (f) Bright-field image of $CaFe_2As_2$ at 100 K, showing a mixture of the tweed and twin domains.[27]

Similar to the $SrFe_2As_2$ samples, the $CaFe_2As_2$ compounds also undergo T–O phase transition at about 170 K and show clear twin domains in the orthorhombic phase, while a new pseudo-periodic structural modulation with a wavelength about 40 nm is observed in the $CaFe_2As_2$ compounds at room temperature. As shown in Fig. 6(e), the modulation waves commonly coexist in many crystals along two equivalent [110] and [1-10] directions of the tetragonal phase, and the two orthogonal modulations overlap to yield an interesting pattern called a 'tweed' structure, as observed in alloys[45] and the Fe-doped $YBa_2Cu_3O_{7-x}$ superconductor.[46] In the low-temperature orthorhombic phase, as shown in Fig. 6(f), the coexistence of a twin lamella and tweed structure in general yields complex microstructure features in the a–b plane of $CaFe_2As_2$. It should be noted that the tweed structures show no visible changes even below the T–O transition, so we conclude that the twinning structures occur within the Fe layers, while the tweed structures are in the Ca layers. The dissimilarities in both electrical resistivity and magnetic susceptibility

between $SrFe_2As_2$ and $CaFe_2As_2$ are likely to be induced from this pseudo-periodic structural modulation.

The correlation between the SDW and superconductivity, as shown in the phase diagram of Fig. 4(a) for a typical 122 system, is considered to be a fundamental issue in Fe-based superconducting materials. In contrast with the 11 system, element doping in superconducting compounds of 1111 and 122 systems often results in structural inhomogeneities and defect structures. TEM observations on the $Ca_{0.5}Sr_{0.5}Fe_{1.74}Co_{0.26}As_2$ superconductor[47] suggest that the inhomogeneous distribution of Sr and Ca could be responsible for the relatively wider superconducting transition often observed in this kind of superconducting material. Recently, measurements of spatially resolved spectroscopy on $NaFe_{1-x}Co_xAs_2$ near the SDW and superconducting phase boundary directly reveal the presence of both SDW and superconducting gaps at the same atomic location, providing compelling evidence for the microscopic coexistence of the SDW and superconducting states.[48]

4. The defect structures in $FeTe_{1-x}Se_x$

The FeTe compound, a typical material in the 11 system, exhibits a structural transition from tetragonal to triclinic phase at low temperature, and a clear AFM transition appears at around 65 K.[49] Superconductivity can be introduced by Se substitution for Te, as discussed above (see the phase diagram in Fig. 4(b)). The $Fe_{1+y}Se$ superconductor ($T_c \approx 8$ K) also shows up visible structural transitions with lowering temperature, and the crystal lattice of this compound has a space group of *P*4/*mmm* at room temperature and undergoes a structural transition to an orthorhombic lattice with space group *Cmma* due to the structural distortions of $FeSe_4$ tetrahedra below 90 K.[50] Moreover, it is noted that the FeSe compounds have a complex phase diagram, as discussed in Refs. [51] and [52], and as a result, impurity phases, such as α-FeSe, Fe_7Se_8, Fe_3O_4, and Fe, often appear in the $Fe_{1+y}Se$ samples.[53,54]

Measurements of the physical properties reveal that all the $FeTe_{1-x}Se_x$ samples are tetragonal paramagnetic metals at high temperatures; on the other hand, this kind of material show a rich variety of physical phenomena at low temperatures, i.e., the SDW ordering for $x < 0.1$, spin glass-like static magnetic ordering for $0.1 < x < 0.3$, and superconductivity for $x > 0.3$.[37] One of the notable phenomena in this system is the presence of a spin glass-like state between the SDW and the superconducting regions, which is considered to be accompanied by the local structural distortion and lattice disorders.[55] Structural measurements using scanning transmission electron microscopy (STEM) and electron energy loss spectroscopy (EELS) on the $Fe_{1+y}Te_{1-x}Se_x$ crystals demonstrate the presence of phase separation and chemical inhomogeneity at the nanoscale.[56] The TEM investigation on the $FeTe_{0.7}Se_{0.3}$ samples shows that areas with a fluctuation in Te concentration around 20% commonly exist in the superconducting compounds. Figure 7 displays a series of experimental data obtained from a well-characterized superconducting sample. Figure 7(b) shows the EELS data taken from line-scanning measurements, as indicated in Fig. 7(a), and the fluctuation in the Te concentration matches well with the simultaneous high angle annular dark field (HAADF) image intensity profile in Fig. 7(c), reflecting the *Z*-contrast alternation following the chemical fluctuation. The alterations in the Fe L_3/L_2 intensity ratio in the EELS spectra also show a clear correlation with the fluctuation in Te concentration, as illustrated in Fig. 7(d), and the Te-rich (poor) regions correspond to lower (higher) L_3/L_2 intensity ratios. A careful analysis of these experimental data suggests alternations in the d-electron occupancy on the Fe ions in different areas, implying a local variation in the magnetic moment in the nanoscale. Moreover, the EELS measurements demonstrate that the valence states of Te and Se could deviate from the nominal valence state of +2, and the substitution of Se with Te leads to a charge transfer and/or an effective doping, as discussed in Ref. [57].

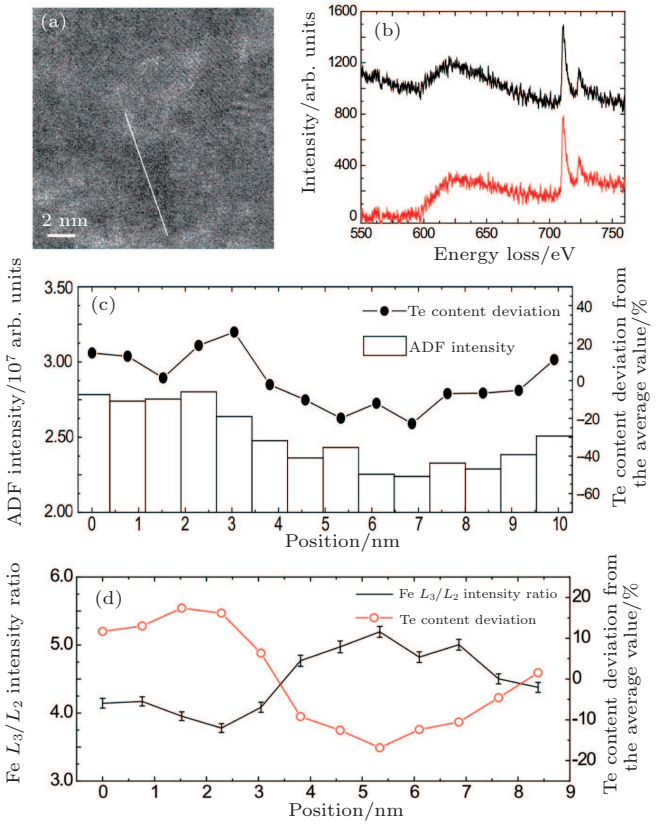


Fig. 7. Phase separation and chemical inhomogeneity in an $FeTe_{0.7}Se_{0.3}$ sample. (b) The red spectrum shows the back ground-subtracted EELS for the Te-$M_{4,5}$ edge along the line in the HAADF image of panel (a), and the black spectrum shows a typical energy loss spectrum. (c) The black dotted curve shows the variation in Te content along the scanning line, and the histogram shows the HAADF intensity recorded simultaneously with the EELS data. (d) The black curve shows the changes in the intensity ratio of the Fe L_3/L_2 white line. The red curve demonstrates that the Te content deviates from the average value.[56]

In addition, other kinds of defect structures, such as twinning domains and grain boundaries, which could affect the superconductivity and critical current density (J_c), have also been examined in $Fe_{1+y}Se$ films using scanning electron microscopy (STM).[58] Twin boundaries aligned 45° to the Fe–Fe bond directions are found to noticeably suppress the superconducting gap, as shown in Fig. 8. The variation in superconductivity is likely caused by the local structural changes in the areas neighboring the twin boundaries. It is also noted in the structural investigations of the iron-based superconductors that the superconductivity T_c depends remarkably on the height from the Se to Fe layer (h_{Se}), and reaches a maximum value at $h_{Se} \approx 1.38$ Å, and decreases abruptly away from this value. In FeSe, h_{Se} ranges from 1.38 Å to 1.45 Å near the twin boundary, and the increase in h_{Se} could suppress T_c at the twin boundaries. Moreover, experimental measurements show that the magnetic vortices are preferentially pinned around the twin boundaries due to the visible changes in the local structure and the degradation of superconductivity.[59]

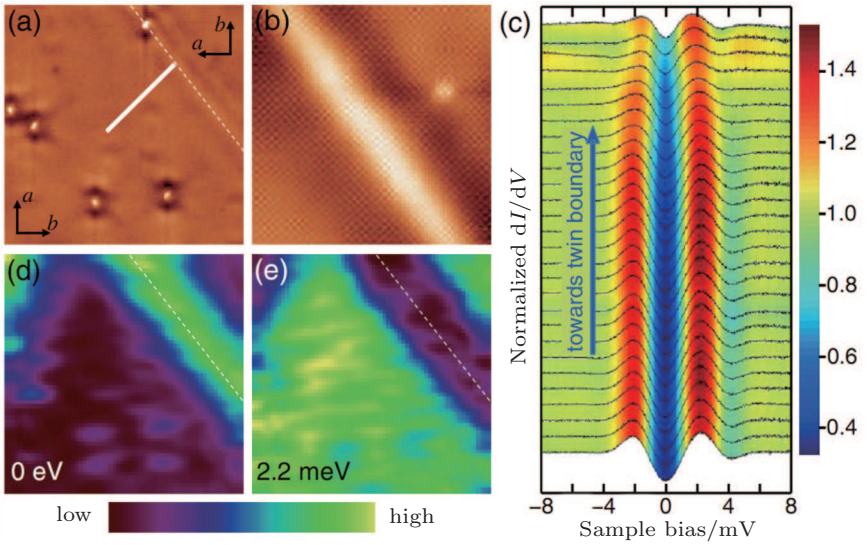


Fig. 8. STM data showing the suppression of superconductivity near a twin boundary in an FeSe film. (a) STM topography with TB indicated by a white dashed line. (b) Atomically resolved topography of the TB. (c) Normalized dI/dV spectra taken along the white solid line in panel (a). (d), (e) Differential conductance maps recorded simultaneously with image (a) at energies of panels (d) 0 and (e) 2.2 meV, respectively.[58]

5. Phase separation and structural transition in $K_{0.8}Fe_{1.6+x}Se_2$

Intercalation of alkali metals into the 122 layered system not only yields superconduction in $A_yFe_{1.6+x}Se_2$, but also results in Fe vacancies in the FeSe layer. Our recent TEM observations demonstrate that certain microstructure phenomena and local structural inhomogeneities are essentially in correlation with the appearance of Fe vacancies in this layer, such as structural modulations from different configurations of vacancy orders, order–disorder transitions, and phase separations in superconducting materials. These microstructural features could fundamentally affect the physical properties, especially the magnetic orders and superconductivity.[60–62]

5.1. Structural modulations and Fe-vacancy ordering in $K_yFe_{1.6+x}Se_2$

The Fe vacancy order and correlated AFM state in this system were first studied in 1987 by means of neutron diffraction on a material with a nominal composition of $TlFe_2S_2$. Two kinds of Fe-vacancy orders were found, but no superconductivity was observed.[63] Based on the structural analysis of (Tl, K)Fe_xSe_2 materials, the Fe-vacancy orders were, respectively, discussed for samples with $x = 1.5$, 1.6, 2.0.[26] In the recent investigations of $A_yFe_{1.6+x}Se_2$ superconductors, microstructural features and superstructure modulations have been extensively studied by means of TEM, STEM,[60,62,64] XRD,[65,66] and neutron scattering,[61,67–72] and the typical superstructures in correlation with the Fe-vacancy orders addressed, e.g., the $\sqrt{5} \times \sqrt{5}$ superstructure (q_1-modulation), $\sqrt{2} \times \sqrt{2}$ superstructure (q_2-modulation), and $\sqrt{2} \times 2\sqrt{2}$ superstructure (q_3-modulation) have been identified as different structural phases in the $A_yFe_{1.6+x}Se_2$ system.

Based on the structural data obtained from the well-characterized samples, we first discuss the fundamental structural features for the q_1- and q_3-modulations. As shown in Fig. 9, our TEM observations and diffraction measurements of $K_yFe_{1.6+x}Se_2$ reveal that the wave vectors for these two modulations can be written as $q_1 = 1/5(3,1,0)$ and $q_3 = 1/4(3,1,0)$ in the notation of the tetragonal 122 structure.[60,73] The chemical composition of q_1-phase is estimated to be $K_{0.8}Fe_{1.6}Se_2$ (the so-called 245 phase), with one Fe vacancy for every five Fe positions. This phase has a space group of $I4/m$ with the lattice parameters $a_1 = b_1 = \sqrt{5}a_s$ and $c_1 = c_s$, where the sublattice parameters are $a_s = 3.913$ Å and $c_s = 14.10$ Å. Simi-

larly, the chemical composition of the q_3-phase can be written as $KFe_{1.5}Se_2$ (the so-called 234 phase). Figure 10(b) shows a structural model for the q_3-phase, which has a space group of *Ibam* with lattice parameters of a_3=2$\sqrt{2}$a$_s$ and $b_3 = \sqrt{2}a_s$. Figure 9 exhibits the electron diffraction patterns and high-resolution TEM/STEM images taken from thin crystals of the q_1- and q_3-modulated phases. In Figs. 9(d) and 9(e), the Fe-vacancy order with visible periodic features can be clearly read out. Moreover, the q_1 modulation and related Fe-vacancy order in $TlFe_{1.6}Se_2$ are directly observed using an aberration-corrected STEM, as shown in Fig. 9(f).[73] This STEM image is taken from a thin area along the [310] zone-axis direction, in which the Fe vacancy can be clearly recognized as dark dots separated by four iron columns. It is also noted that the Fe ions in both the $K_2Fe_4Se_5$ and $K_2Fe_3Se_4$ phases have a valence state of Fe^{2+}, and therefore these two phases are expected to exhibit semiconducting/insulating properties in agreement with the experimental results.

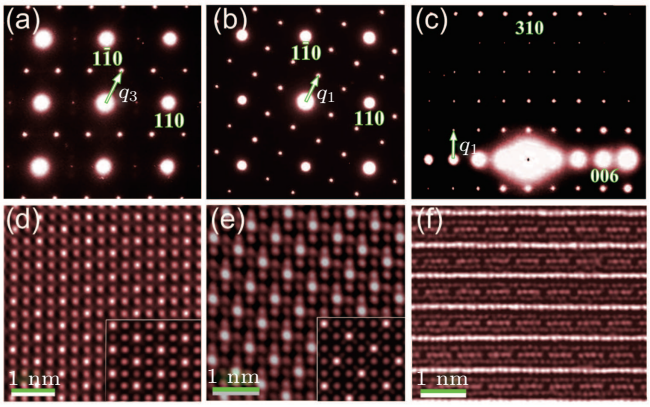


Fig. 9. Electron diffraction patterns and high-resolution TEM images taken along relevant directions. The electron diffraction patterns showing (a) the $q_3 = 1/4(3,1,0)$ modulation for $K_2Fe_3Se_4$, (b) the $q_1 = 1/5(3,1,0)$ modulation for $K_2Fe_4Se_5$, and (c) the q_1 modulation observed along the [130] direction. The HRTEM image illustrating the ordered arrangement of iron vacancies for (d) the 234 phase and (e) the 245 phase. (f) High angle annular dark field (HADDF) image taken along the [310] zone-axis direction directly illustrating the iron vacancies as the dark dots, which is consistent with the diffraction pattern in panel (e).[60,73]

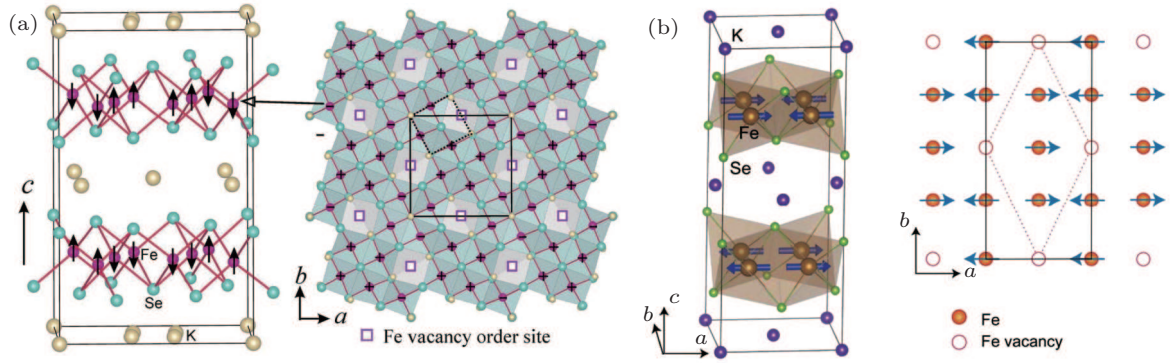


Fig. 10. Crystal and magnetic structures for (a) $K_{0.8}Fe_{1.6}Se_2$ and (b) $KFe_{1.5}Se_2$. The Fe-vacancy orders and layered structural features are clearly illustrated.[61,71]

The magnetic structures in association with different Fe-vacancy orders, including the q_1 and q_3 phases, were discussed with theoretical calculations.[74] Neutron diffraction[49] from the $K_2Fe_4Se_5$ crystal shows an AFM transition at $T_N \approx 559$ K below the Fe-vacancy order-disorder transition at $T_S \approx 578$ K. The magnetic unit cell, as depicted in Fig. 10(a), is the same as the $K_2Fe_4Se_5$ crystal unit cell with a low occupancy on one Fe site surrounded by a square of four fully occupied Fe sites. The Fe magnetic moments form a collinear AFM structure with the c axis being the easy magnetic axis, and the magnetic moment of Fe ($\sim 3.31\ \mu_B$) obtained at 11 K is the largest among all iron pnictide and chalcogenide superconductors. Other neutron diffraction studies on $Cs_yFe_{2-x}Se_2$ and $Rb_yFe_{1.6+x}Se_2$ have also revealed the similar phase transition and AFM structure.[67–70] Magnetic ordering associated with the Fe-vacancy order have also been observed in the $KFe_{1.5}Se_2$ phase,[71] as clearly illustrated in Fig. 10(b). The magnetic moment of Fe in the present case is estimated to be about

2.8 μ_B, which is compatible with the theoretical data.[74]

5.2. Phase separation in the $A_{0.8}Fe_{1.6+x}Se_2$ superconducting system

The phase separation phenomenon in $A_{0.8}Fe_{1.6+x}Se_2$ superconductors has been directly observed using TEM,[60,62] scanning electron microscopy (SEM),[75,76] STM,[77] X-ray diffraction,[78,79] and neutron scattering.[67–70] A careful structural analysis demonstrates that notable microstructural features in the present system arise fundamentally from the phase separations at both microscale and nanoscale. Furthermore, Mössbauer spectroscopy,[80] Raman spectroscopy,[81] and angle resolved photoemission spectroscopy[82] also give strong evidence for the presence of phase separation in this superconducting system, in which about 80%–90% of the volume of the sample exhibits antiferromagnetic order, and a volume fraction of about 10%–20% could be attributed to superconductivity at low temperature.

Direct observations of the atomic structural features in the phase separated state of $K_yFe_{1.6+x}Se_2$ superconductors have been performed by high-resolution TEM (HRTEM).[60,62] Remarkable microstructure phenomena have been clearly observed, such as Fe-vacancy ordering, structural inhomogeneity, and phase-separation layers along the c-axis direction. As shown in Fig. 11, the SADPs and HRTEMs for $K_{0.8}Fe_{1.6+x}Se_2$ superconductors reveal the coexistence of the $K_2Fe_4Se_5$ phase with another q_2 phase on the nanometer scale. This phase separation phenomenon can be clearly observed in the a–b plane and along the c axis. The superstructure spots in the SADPs show that the q_2 phase has a modulated vector of $q_2 = 1/2(1,1,0)$. Further study suggests that this q_2 phase is correlated with the superconductivity in the present system.

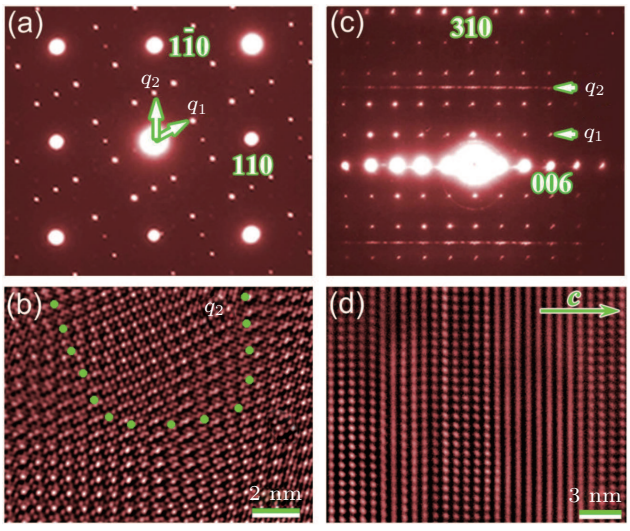


Fig. 11. Phase separation between the q_1 phase ($K_2Fe_4Se_5$) and q_2 phase with $q_2 = 1/2(1,1,0)$ at the nanoscale in a $K_{0.8}Fe_{1.7}Se_2$ superconductor. The SADPs and corresponding HRTEM images taken from [(a), (b)] [001] and [(c), (d)] [310] zone-axis directions illustrate the nanoscale phase separation between the $K_2Fe_4Se_5$ and q_2 phases.[60,62]

In order to clearly view the microstructure features in the phase separated states for this layered system, a series of well-characterized $K_{0.8}Fe_{1.6+x}Se_2$ single-crystal samples were prepared for structural investigations.[62] Measurements of resistivity and magnetic susceptibility show that $K_{0.8}Fe_{1.6}Se_2$ exhibits the semiconducting property in the low-temperature range. With the increase in Fe content, the $K_{0.8}Fe_{1.6+x}Se_2$ compounds exhibit superconductivity for x larger than 0.06. The transition between the AFM phase $K_{0.8}Fe_{1.6}Se_2$ and the superconductor is likely in association with a mixed phase in which an obvious structural inhomogeneity can often be observed. In our experimental investigations, it is noted that SEM/EDX observations unambiguously reveal the visible alterations of the chemical compositions on $K_{0.8}Fe_{1.76}Se_2$ superconducting crystals at the micron/nano-scales,[75] and Fe-rich regions can be clearly distinguished in the SEM secondary electron images. A careful analysis suggests that the most remarkable microstructure features in the present system are the micro-scale stripe-like patterns appearing in all the superconducting samples, as clearly shown in Fig. 12. The density of the stripes increases progressively with the increase in Fe content. These striped patterns also show a visible correlation with the anisotropic assembly of superconducting domains along the [110] and [1-10] directions in the a–b plane. Moreover, the three-dimensional structural features of the phase separated states have also been examined, and a structural framework arising from the stacking of the macro stripes can be clearly recognized along the

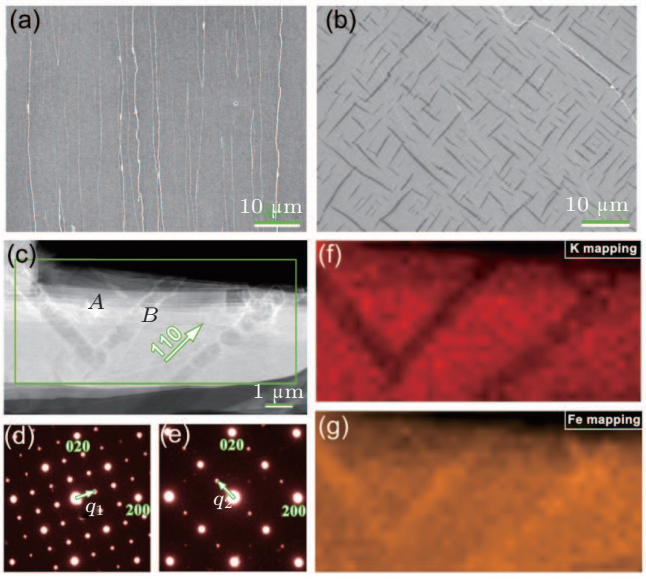


Fig. 12. TEM/STEM images showing phase separation at the microscale. The striped pattern of the q_2 phase is embedded in the matrix of the semiconducting $K_2Fe_4Se_5$ phase. SEM images of the a–b plane in $K_{0.8}Fe_{1.6+x}Se_2$ samples with (a) $x = 0$, (b) 0.06 demonstrate that the striped pattern emerges along with the appearance of superconductivity as the Fe content increases. (c) STEM image of $K_{0.8}Fe_{1.7}Se_2$ along the c-axis direction shows the striped pattern with darker contrast along the [110] and [1$\bar{1}$0] directions. SAEDPs taken from a light A area (d) with a modulated vector of $q_1 = 1/5[a^* + 3b^*]$ and the striped B area (e) with modulation of $q_2 = 1/2[a^* + b^*]$. Elemental mapping of the rectangular area for (f) the K element and (g) the Fe element illustrates the higher Fe concentration for the q_2 phase.[62]

[113] direction. As presented in Fig. 12, the Fe-poor domains are dominant by the known AFM 245 phase with $q_1 = 1/5(3,1,0)$, and the superstructure phase with the modulation of $q_2 = 1/2(1,1,0)$ is mostly concentrated in the Fe-rich striped areas. The q_2 phase with the composition of $K_{0.5}Fe_2Se_2$ and an expanded c axis compared with the 245 phase is considered to be the superconducting phase,[62,78] which is thought to be induced by the ordered arrangement of K vacancies. In addition to the notable striped structures, the nanoscale phase separation mentioned in the previous literature also appears around and within the striped areas in the superconducting materials.

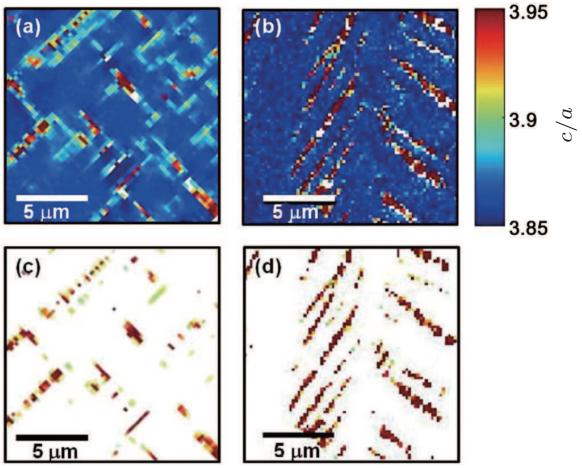


Fig. 13. HR-EBSD analysis shows the variation in the c/a ratio for samples with nominal composition (a) $Cs_{0.8}Fe_{1.9}Se_2$ ($T_c \sim 27$ K) and (b) $Cs_{0.87}Fe_{2.04}Se_2$ ($T_c \sim 23$ K). (c), (d) Regions with $c/a > 3.9$ refer to the minority phase.[76]

The phase separation nature in other related materials has also been studied. For instance, high-resolution electron backscatter diffraction (HR-EBSD) mapping of $Cs_xFe_{2-y}Se_2$ has been used to analyze the local variations in the composition and lattice parameters on a micron scale in the phase separated state.[76] The experimental results demonstrate that the phase separated state containing an Fe-rich minor phase is distributed as a plate-like morphology throughout the crystal in the matrix of the q_1-superstructing phase, which is inconsistent with our experimental results. Figure 13 shows the HR-EBSD maps for $Cs_{0.8}Fe_{1.9}Se_2$ and $Cs_{0.87}Fe_{2.04}Se_2$ with $T_c = 27$ K and 23 K, respectively, illustrating a relatively larger c/a ratio in the minor phase than that of the matrix. An X-ray study on this sample found a 5% increase of the c/a ratio corresponding to a 2.4% expanded c axis and 2.4% contracted a axis.[83] The authors explained these changes as a result of further nanoscale phase separation within the Fe-rich minor region, and this microstructure phenomenon was also observed in our TEM study.

Recently, structural studies on $K_{0.8}Fe_{1.6+x}Se_2$ superconductors using high-resolution synchrotron and single-crystal X-ray diffraction[79] identified four distinct phase: the well-known semiconducting $K_2Fe_4Se_5$ phase (q_1 phase), a metallic superconducting phase $K_xFe_2Se_2$ (q_2 phase), with x ranging from 0.38 to 0.58, an insulator phase $KFe_{1.6}Se_2$ with no vacancy ordering, and an oxidized $K_{0.51}Fe_{1.7}Se_2$. Based on these results, it was also stated that additional Fe in $K_2Fe_4Se_5$ could induce a distinct $K_xFe_2Se_2$ precipitate, which is consistent with the dots/stripes found in our microstructure observations. Due to the complexity of the $K_{0.8}Fe_{1.6+x}Se_2$ superconductors, certain structural and physical properties for either the parent or superconducting phase are still under debate. Scanning tunneling microscopy and spectroscopy measurements on $K_{0.8}Fe_{1.6+x}Se_2$ superconductors suggest a stoichiometric metal KFe_2Se_2 with $\sqrt{2}\times\sqrt{2}$ charge ordering as the parent compound,[84] and superconductivity is induced in KFe_2Se_2 by either Se vacancies (e.g., superconducting KFe_2Se_{2-z} with Se vacancies) or interaction with the AFM $K_2Fe_4Se_5$ compound (superconducting KFe_2Se_2 with $\sqrt{2}\times\sqrt{5}$ charge ordering). NMR measurements[85] have concluded that the superconducting phase might have the formula $A_{0.3}Fe_2Se_2$ (A = K, Rb).

5.3. Phase transitions in $K_2Fe_4Se_5$ and $K_{0.8}Fe_{1.6+x}Se_2$ superconductors

Neutron diffraction measurements on a $K_2Fe_4Se_5$ single crystal demonstrated that the $K_2Fe_4Se_5$ phase exhibits an AFM order in correlation with an Fe-vacancy ordering transition at about 558 K.[61] In order to directly reveal the alteration of the microstructure in association with the Fe-vacancy ordering, we performed a series of *in-situ* TEM and X-ray diffraction experiments on $K_2Fe_4Se_5$ samples[72] in the temperature range from 300 K up to 800 K. Figure 14(a) schematically shows the changes in resistivity and magnetic susceptibility for $K_yFe_{2-x}Se_2$ at high temperatures, as extensively discussed in Ref. [86]. The $K_2Fe_4Se_5$ phase undergoes AFM transition following Fe-vacancy ordering and often shows visible resistivity anomalies at high temperatures. Figure 14(b) exhibits a series of selected-area electron diffraction patterns taken along the [001] zone-axis direction of the $K_2Fe_4Se_5$ crystal, illustrating the visible changes in the superstructure with the increase in temperature. This *in-situ* TEM observation clearly demonstrates that the $K_2Fe_4Se_5$ phase contains a notable superstructure modulation (q_1) at 300 K and undergoes a transformation, via an intermediate phase with a short-range order, toward an Fe-vacancy disordered state. The diffused superstructure spots observed above 500 K suggest a short-range order possibly resulting from an intermediate state short coherent length, similar to that discussed with regard to SrNdCaCuOF.[87] The high-temperature structure can be well characterized by a 122

structure with space group *I*4/*mmm* and lattice parameters $a = b = 3.913$ Å, $c = 14.10$ Å. Moreover, our powder X-ray diffraction on a $K_2Fe_4Se_5$ sample also reveals clear the structural changes in the temperature range from 300 K to 600 K, as shown in Fig. 14(c). It is recognizable that the peaks corresponding to the superstructures marked by asterisks disappear at temperatures above 600 K. These results are in good agreement with the *in-situ* TEM observations.

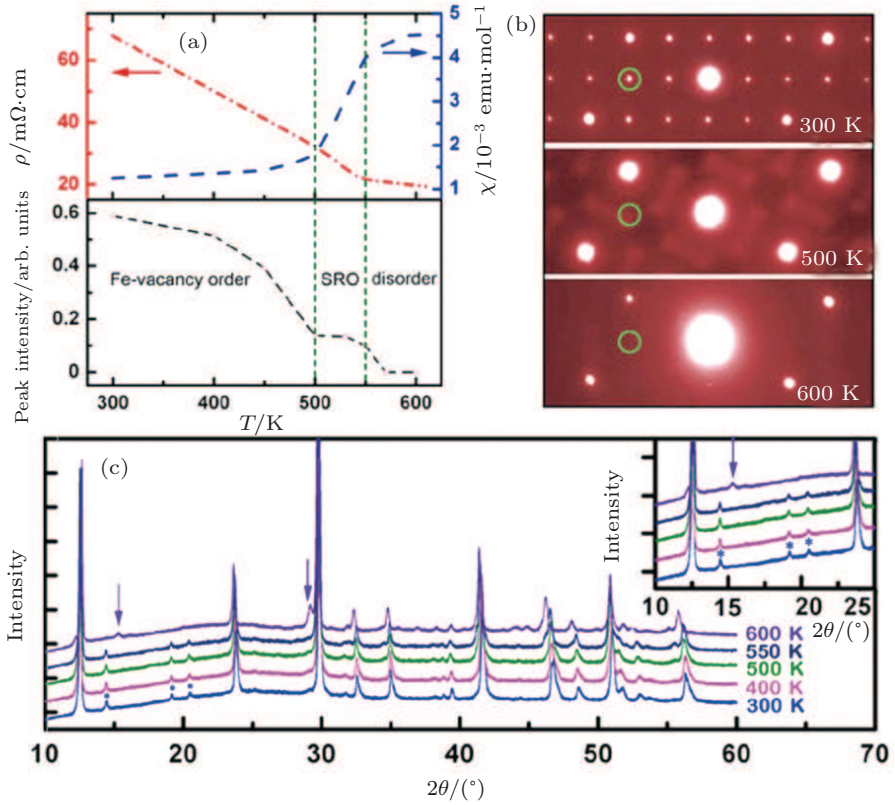


Fig. 14. (a) Schematic illustration of alterations in resistivity and magnetic susceptibility for $K_{0.8}Fe_{1.6}Se_2$ at high temperatures. The structural changes are observed in TEM and XRD measurements. (b) Electron diffraction patterns at temperatures from 300 K to 600 K. (c) The XRD of $K_{0.8}Fe_{1.6}Se_2$ polycrystalline samples at different temperatures; the two arrows mark the (001) and (011) peaks of FeSe splitting at around 600 K.[72]

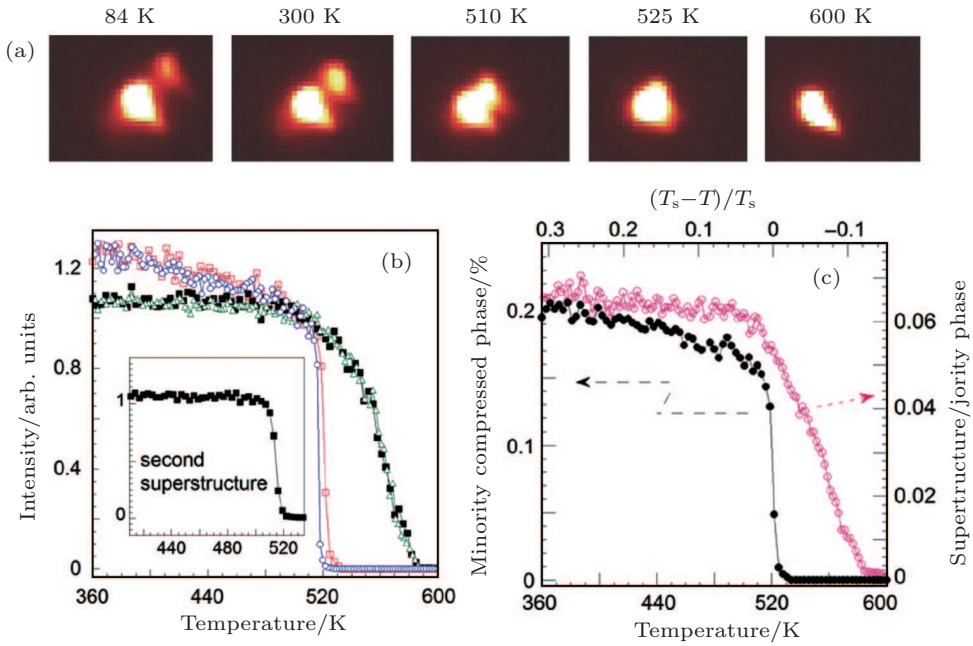


Fig. 15. X-ray diffraction data of $K_{0.8}Fe_{1.6+x}Se_2$ showing the intrinsic phase separation. (a) The temperature evolution of (200) peaks; the splitting of the peak at low temperatures gives evidence for the appearance of the majority in-plane expanded $K_2Fe_4Se_5$ phase and the minority in-plane compressed q_2 superconducting phase. (b) Temperature evolution of the q_1 and q_2 superstructure satellite intensity during the heating and cooling runs. (c) The variation in the probability of the q_2 phase around the phase separation temperature and the temperature variation of the ratio between the intensity of q_1 satellites and basic diffraction spots.[88]

The phase separation in $K_{0.8}Fe_{1.6+x}Se_2$ superconductors as an important issue has also been observed using *in-situ* synchrotron radiation in the transmission mode,[88] demonstrating a clear phase separation between two competing phases: the majority q_1 phase with an in-plane expanded lattice and a minority non-magnetic q_2 phase with a compressed in-plane lattice. The high-temperature structure (above 600 K) is found to be tetragonal 122 type, as discussed in the above context. As shown in Fig. 15, the q_1 phase appears at 580 K, which is consistent with our *in-situ* TEM and neutron diffraction results. With a further decrease in temperature, a new q_2 phase, which merges with the q_1 phase, appears at 520 K. The two phases are assigned to a lattice-electronic instability, and $K_{0.8}Fe_{1.6}Se_2$ is considered as a typical system tuned at the Lifshitz critical point with an electronic topological transition that yields a multi-gap superconductor.[88]

6. Summary

In this article, we have demonstrated the complex microstructural phenomena in Fe-based high-T_c superconductors. The richness and complexity of the microstructural phenomena are truly remarkable. We focused on the structural phase transitions, defect structures, and the chemical and structural inhomogeneities that commonly appear in a variety of Fe-based superconducting families. In particular, we considered the crystal structural features for different superconducting systems, the local structural distortion in the Fe_2Pn_2 (Pn = P, As, Sb) or Fe_2Ch_2 (Ch = S, Se, Te) blocks, and the structural phase transition. In FeTe(Se) (11 family), the superconductivity and chemical and structural defects were investigated in the related materials. Local structural analysis on the twinning boundaries clearly reveals the effects of structural changes on superconductivity. In $A_{0.8}Fe_{1.6+x}Se_2$ (A = K, Rb) superconducting materials, the phase separated states on the micro and nano scales were evidently observed. The q_2 phase with a composition of $K_yFe_2Se_2$ ($y \approx 0.5$) is considered to be the superconducting phase.

References

[1] Kamihara Y, Hiramatsu H, Hirano M, Kawamura R, Yanagi H, Kamiya T and Hosono H 2006 *J. Am. Chem. Soc.* **128** 10012

[2] Kamihara Y, Watanabe T, Hirano M and Hosono H 2008 *J. Am. Chem. Soc.* **130** 3296

[3] Chen X H, Wu T, Wu G, Liu R H, Chen H and Fang D F 2008 *Nature* **453** 761

[4] Takahashi H, Igawa K, Arii K, Kamihara Y, Hirano M and Hosono H 2008 *Nature* **453** 376

[5] Kito H, Eisaki H and Iyo A 2008 *J. Phys. Soc. Jpn.* **77** 063707

[6] Wang C, Li L J, Chi S, Zhu Z W, Ren Z, Li Y K, Wang Y T, Lin X, Luo Y K, Jiang S, Xu X F, Cao G H and Xu Z A 2008 *Europhys. Lett.* **83** 67006

[7] Ren Z A, Lu W, Yang J, Yi W, Shen X L, Li Z C, Che G C, Dong X L, Sun L L, Zhou F and Zhao Z X 2008 *Chin. Phys. Lett.* **25** 2215

[8] Sefat A S, Jin R, McGuire M A, Sales B C, Singh D J and Mandrus D 2008 *Phys. Rev. Lett.* **101** 117004

[9] Rotter M, Tegel M and Johrendt D 2008 *Phys. Rev. Lett.* **101** 107006

[10] Ronning F, Klimczuk T, Bauer E D, Volz H and Thompson J D 2008 *J. Phys.: Condens. Matter* **20** 322201

[11] Chen G F, Li Z, Li G, Hu W Z, Dong J, Zhang X D, Zheng P, Wang N L and Luo J L 2008 *Chin. Phys. Lett.* **25** 3403

[12] Wang X C, Liu Q Q, Lü Y X, Gao W B, Yang L X, Yu R C, Li F Y and Jin C Q 2008 *Solid State Commun.* **148** 538

[13] Pitcher M J, Parker D R, Adamson P, Herkelrath S J C, Boothroyd A T, Ibberson R M, Brunelli M and Clarke S J 2008 *Chem. Commun.* **45** 5918

[14] Deng Z, Wang X C, Liu Q Q, Zhang S J, Lü Y X, Zhu J L, Yu R C and Jin C Q 2009 *Europhys. Lett.* **87** 37004

[15] Tapp J H, Tang Z, Lv B, Sasmal K, Lorenz B, Chu P C W and Guloy A M 2008 *Phys. Rev. B* **78** 060505

[16] Hsu F C, Luo J Y, Yeh K W, Chen T K, Huang T W, Wu P M, Lee Y C, Huang Y L, Chu Y Y, Yan D C and Wu M K 2008 *Proc. Natl. Acad. Sci. USA* **105** 14262

[17] Sales B C, Sefat A S, McGuire M A, Jin R Y, Mandrus D and Mozharivskyj Y 2009 *Phys. Rev. B* **79** 094521

[18] Ogino H, Matsumura Y, Katsura Y, Ushiyama K, Horii S, Kishio K and Shimoyama J I 2009 *Supercond. Sci. Technol.* **22** 075008

[19] Ogino H, Shimizu Y, Ushiyama K, Kawaguchi N, Kishio K and Shimoyama J 2010 *Appl. Phys. Express* **3** 063103

[20] Zhu X, Han F, Mu G, Cheng P, Shen B, Zeng B and Wen H H 2009 *Phys. Rev. B* **79** 220512

[21] Chen G F, Xia T L, Yang H X, Li J Q, Zheng P, Luo J L and Wang N L 2009 *Supercond. Sci. Technol.* **22** 072001

[22] Guo J, Jin S, Wang G, Wang S, Zhu K, Zhou T, He M and Chen X 2010 *Phys. Rev. B* **82** 180520

[23] Wang A F, Ying J J, Yan Y J, Liu R H, Luo X G, Li Z Y, Wang X F, Zhang M, Ye G J, Cheng P, Xiang Z J and Chen X H 2011 *Phys. Rev. B* **83** 060512

[24] KrztonMaziopa S, Shermadini Z, Pomjakushina E, Pomjakushin V, Bendele M, Amato A, Khasanov R, Luetkens H and Conder K 2011 *J. Phys.: Condens. Matter* **23** 052203

[25] Wang H D, Dong C H, Li Z J, Mao Q H, Zhu S S, Feng C M, Yuan H Q and Fang M H 2011 *Europhys. Lett.* **93** 47004

[26] Fang M H, Wang H D, Dong C H, Li Z J, Feng C M, Chen J and Yuan H Q 2011 *Europhys. Lett.* **94** 27009

[27] Ma C, Yang H X, Tian H F, Shi H L, Lu J B, Wang Z W, Zeng L J, Chen G F, Wang N L and Li J Q 2009 *Phys. Rev. B* **79** 060506

[28] Kastner M A, Birgeneau R J, Shirane G and Endoh Y 1998 *Rev. Mod. Phys.* **70** 897

[29] Dai P C, Hu J P and Elbio D 2012 *Nat. Phys.* **8** 709

[30] Cruz C de la, Huang Q, Lynn J W, Li J Y, Ratcliff W, Zarestky J L, Mook H A, Chen G F, Luo J L, Wang N L and Dai P C 2008 *Nature* **453** 899

[31] Zhao J, Huang Q, Cruz C de la, Li S L, Lynn J W, Chen Y, Green M A, Chen G F, Li G, Li Z, Luo J L, Wang N L and Dai P C 2008 *Nat. Mater.* **7** 953

[32] Li S, Cruz C de la, Huang Q, Chen Y, Lynn J W, Hu J, Huang Y L, Hsu F C, Yeh K W, Wu M K and Dai P C 2009 *Phys. Rev. B* **79** 054503

[33] Ma F, Ji W, Hu J, Lu Z Y and Xiang T 2009 *Phys. Rev. Lett.* **102** 177003

[34] Wen H H and Li S 2011 *Ann. Rev. Condens. Matter Phys.* **2** 121

[35] Luetkens H, Klauss H H, Kraken M, Litterst F J, Dellmann T, Klingeler R, Hess C, Khasanov R, Amato A, Baines C, Kosmala M, Schumann O J, Braden M, Hamann-Borrero J, Leps N, Kondrat A, Behr G, Werner J and Büchner B 2009 *Nat. Mater.* **8** 305

[36] Nandi S, Kim M G, Kreyssig A, Fernandes R M, Pratt D K, Thaler A, Ni N, Bud'ko S L, Canfield P C, Schmalian J, McQueeney R J and Goldman A I 2010 *Phys. Rev. Lett.* **104** 057006

[37] Katayama N, Ji S, Louca D, Lee S, Fujita M, Sato T J, Wen J, Xu Z, Gu G, Xu G, Lin Z, Enoki M, Changi S, Yamada K and Tranquada J M 2010 *J. Phys. Soc. Jpn.* **79** 113702

[38] Johrendt D, Hosono H, Hoffmann R D and Pöttgen R 2011 *Z. Kristallogr.* **226** 435

[39] Lynn J W and Dai P C 2009 *Physica C* **469** 469

[40] Oh H, Moon J, Shin D H, Moon C Y and Choi H J 2011 *Progress in Superconductivity* **13** 65

[41] Ogino H, Sato S, Kishio K, Shimoyama J, Tohei T and Ikuhara Y 2010 *Appl. Phys. Lett.* **97** 072506

[42] Dong J, Zhang H J, Xu G, Li Z, Li G, Hu W Z, Wu D, Chen G F, Dai X, Luo J L, Fang Z and Wang N L 2008 *Europhys. Lett.* **83** 27006

[43] Shi H L, Yang H X, Tian H F, Ma C, Lu J B, Wang Z W, Qin Y B, Song Y J and Li J Q 2011 *J. Phys. Chem. Solids* **72** 420

[44] Muto S, Takeda S, Oshima R and Fujita F E 1989 *J. Phys.: Condens. Matter* **1** 9971

[45] Zhao J, Ratcliff W, Lynn J W, Chen G F, Luo J L, Wang N L, Hu J and Dai P 2008 *Phys. Rev. B* **78** 140504

[46] Zhu Y, Suenaga M and Moodenbaugh A R 1991 *Ultramicroscopy* **37** 341

[47] Shi H L, Yang H X, Tian H F, Ma C, Lu J B, Wang Z W and Li J Q 2010 *J. Supercond. Nov. Magn.* **23** 749

[48] Cai P, Zhou X D, Ruan W, Wang A F, Chen X H, Lee D H and Wang Y Y 2013 *Nature Commun.* **4** 1596

[49] Liu T J, Hu J, Qian B, Fobes D, Mao Z Q, Bao W, Reehuis M, Kimber S A J, Prokes K, Matas S, Argyriou D N, Hiess A, Rotaru A, Pham H, Spinu L, Qiu Y, Thampy V, Savici A T, Rodriguez J A and Broholm C 2010 *Nat. Mater.* **9** 718

[50] Margadonna S, Takabayashi Y, McDonald M T, Kasperkiewicz K, Mizuguchi Y, Takano Y, Fitch A N, Suard E and Prassides K 2008 *Chem. Commun.* **43** 5607

[51] Okamoto H 1991 *J. Phase Equilib.* **12** 383

[52] McQueen T M, Huang Q, Ksenofontov V, Felser C, Xu Q, Zandbergen H, Hor Y S, Allred J, Williams A J, Qu D, Checkelsky J, Ong N P and Cava R J 2009 *Phys. Rev. B* **79** 014522

[53] Patel U, Hua J, Yu S H, Avci S, Xiao Z L, Claus H, Schlueter J, Vlasko-Vlasov V V, Welp U and Kwok W K 2009 *Appl. Phys. Lett.* **94** 082508

[54] Hu R, Lei H, Abeykoon M, Bozin E S, Billinge S J L, Warren J B, Siegrist T and Petrovic C 2011 *Phys. Rev. B* **83** 224502

[55] Katayama N, Ji S, Louca D, Lee S H, Fujita M, Sato T J, Wen J S, Xu Z J, Gu G D, Xu G, Lin Z W, Enoki M, Chang S, Yamada K and Tranquada J M 2010 *J. Phys. Soc. Jpn.* **79** 113702

[56] Hu H F, Zuo J M, Wen J S, Xu Z J, Lin Z W, Li Q, Gu G, Park W K and Greene L H 2011 *New J. Phys.* **13** 053031

[57] Louca D, Horigane K, Llobet A, Arita R, Ji S, Katayama N, Konbu S, Nakamura K, Koo T Y, Tong P and Yamada K 2010 *Phys. Rev. B* **81** 134524

[58] Song C L, Wang Y L, Jiang Y P, Wang L L, He K, Chen X, Hoffman J E, Ma X C and Xue Q K 2012 *Phys. Rev. Lett.* **109** 137004

[59] Lairson B M, Streiffer S K and Bravman J C 1990 *Phys. Rev. B* **42** 10067

[60] Wang Z, Song Y J, Shi H L, Wang Z W, Chen Z, Tian H F, Chen G F, Guo J G, Yang H X and Li J Q 2011 *Phys. Rev. B* **83** 140505

[61] Bao W, Huang Q, Chen G F, Green M A, Wang D M, He J B, Wang X Q and Qiu Y 2011 *Chin. Phys. Lett.* **28** 086104

[62] Wang Z W, Wang Z, Song Y J, Ma C, Cai Y, Chen Z, Tian H F, Yang H X, Chen G F and Li J Q 2012 *J. Phys. Chem. C* **116** 17847

[63] Klepp K and Boller H 1978 *Monatsh. Chem.* **109** 1049

[64] Kazakov S M, Abakumov A M, González S, Perez-Mato J M, Ovchinnikov A V, Roslova M V, Boltalin A I, Morozov I V, Antipov E V and Van Tendeloo G 2011 *Chem. Mater.* **23** 4311

[65] Zavalij P, Bao W, Wang X F, Ying J J, Chen X H, Wang D M, He J B, Wang X Q, Chen G F, Hsieh P Y, Huang Q and Green M A 2011 *Phys. Rev. B* **83** 132509

[66] Bacsa J, Ganin A Y, Takabayashi Y, Christensen K E, Prassides K, Rosseinsky M J and Claridge J B 2011 *Chem. Sci.* **2** 1054

[67] Wang M, Wang M Y, Li G N, Huang Q, Li C H, Tan G T, Zhang C L, Cao H B, Tian W, Zhao Y, Chen Y C, Lu X Y, Sheng B, Luo H Q, Li S L, Fang M H, Zarestky J L, Ratcliff W, Lumsden M D, Lynn J W and Dai P C 2011 *Phys. Rev. B* **84** 094504

[68] Bao W, Li G N, Huang Q, Chen G F, He J B, Green M A, Qiu Y, Wang D M and Luo J L 2013 *Chin. Phys. Lett.* **30** 027402

[69] Ye F, Chi S, Bao W, Wang X F, Ying J J, Chen X H, Wang H D, Dong C H and Fang M H 2011 *Phys. Rev. Lett.* **107** 137003

[70] Pomjakushina E V, Krzton-Maziopa A, Conder K, Chernyshov D, Svitlyk V and Shermadini Z 2011 *Phys. Rev. B* **83** 144410

[71] Zhao J, Cao H, Bourret-Courchesne E, Lee D H and Birgeneau R J 2012 *Phys. Rev. Lett.* **109** 267003

[72] Song Y J, Wang Z, Wang Z W, Shi H L, Chen Z, Tian H F, Yang H X and Li J Q 2011 *Europhys. Lett.* **95** 37007

[73] May A F, McGuire M A, Cao H B, Sergueev I, Cantoni C, Chakoumakos B C, Parker D S and Sales B C 2012 *Phys. Rev. Lett.* **109** 077003

[74] Yan X W, Gao M, Lu Z Y and Xiang T 2011 *Phys. Rev. Lett.* **106** 087005

[75] Hu R, Mun E D, Ryan D H, Cho K, Kim H, Hodovanets H, Straszheim W E, Tanatar M A, Prozorov R, Rowan-Weetaluktuk W N, Cadogan J M, Altarawneh M M, Mielke C H, Zapf V S, Bud'ko S L and Canfield P C 2011 arXiv: 1201. 0953

[76] Speller S C, Britton T B, Hughes G M, Krzton-Maziopa A, Pomjakushina E, Conder K, Boothroyd A T and Grovenor C R M 2012 *Supercond. Sci. Technol.* **25** 084023

[77] Li W, Ding H, Deng P, Chang K, Song C, He K, Wang L, Ma X, Hu J P, Chen X and Xue Q K 2012 *Nat. Phys.* **8** 126

[78] Ricci A, Poccia N, Campi G, Joseph B, Arrighetti G, Barba L, Reynolds M, Burghammer M, Takeya H, Mizuguchi Y, Takano Y, Colapietro M, Saini N L and Bianconi A 2011 *Phys. Rev. B* **84** 060511

[79] Shoemaker D P, Chung D Y, Claus H, Francisco M C, Avci S, Llobet A and Kanatzidis M G 2012 *Phys. Rev. B* **86** 184511

[80] Ksenofontov V, Wortmann G, Medvedev S A, Tsurkan V, Deisenhofer J, Loidl A and Felser C 2011 *Phys. Rev. B* **84** 180508

[81] Zhang A M, Xiao J H, Li Y S, He J B, Wang D M, Chen G F, Normand B, Zhang Q M and Xiang T 2012 *Phys. Rev. B* **85** 214508

[82] Chen F, Xu M, Ge Q Q, Zhang Y, Ye Z R, Yang L X, Jiang J, Xie B P, Che R C, Zhang M, Wang A F, Chen X H, Shen D W, Hu J P and Feng D L 2011 *Phys. Rev. X* **1** 021020

[83] Bosak A, Svitlyk V, Krzton-Maziopa A, Pomjakushina E, Conder K, Pomjakushin V, Popov A, Sanctis D and Chernyshov D 2012 arXiv: 1112.2569

[84] Li W, Ding H, Li Z, Deng P, Chang K, He K, Ji S H, Wang L L, Ma X C, Hu J P, Chen X and Xue Q K 2012 *Phys. Rev. Lett.* **109** 057003

[85] Texier Y, Deisenhofer J, Tsurkan V, Loidl A, Inosov D S, Friemel G and Bobroff J 2012 *Phys. Rev. Lett.* **108** 237002

[86] Liu R H, Luo X G, Zhang M, Wang A F, Ying J J, Wang X F, Yan Y J, Xiang Z J, Cheng P, Ye G J, Li Z Y and Chen X H 2011 *Europhys. Lett.* **94** 27008

[87] Li J Q, Isobe M, Takayama-Muromachi E and Matsui Y 1997 *J. Appl. Phys.* **81** 1628

[88] Ricci A, Poccia N, Joseph B, Arrighetti G, Barba L, Plaisier J, Campi G, Mizuguchi Y, Takeya H, Takano Y, Saini N L and Bianconi A 2011 *Supercond. Sci. Technol.* **24** 082002